



Ultralight and thermal insulation carbon foam/SiO₂ aerogel composites

Yang Liu¹ · Zhaofeng Chen¹ · Junxiong Zhang¹ · Sufen Ai² · Hao Tang¹

Published online: 11 February 2019
© Springer Science+Business Media, LLC, part of Springer Nature 2019

Abstract

In this study, carbon foam (CF) and SiO₂ aerogel composite were prepared by the sol–gel method under a circumstance of the atmospheric drying process. The Pyrolysis mechanism of carbon foam was investigated through thermal gravimetric analysis and Fourier transform infrared spectroscopy (FTIR). Carbon foam having ultralight properties with a density of 5.44 kg/m³, functions as a skeleton to support the composite. The maximum compressive stress measured for CF/SiO₂ aerogel composite was about 1.0 MPa. At room temperature, the measured thermal conductivities of the CF and CF/SiO₂ aerogel composite were 0.035 W/m K and 0.024 W/m K, while at 300 °C, it was reported to be 0.120 W/m K and 0.057 W/m K. Aerogel filled in carbon foam cells have significantly reduced the gaseous thermal conductivity of the prepared composite.

Keywords Carbon foam · SiO₂ aerogel · Composite · Thermal conductivity

1 Introduction

In recent years, various techniques and methodologies have been adopted for the identification of lightweight materials having low thermal conductivity. For this purpose, researchers have focused on integrating superinsulation materials on ultralight and thermal insulating carbon foams [1]. These carbon foams are a highly porous material with a three-dimensional network, along with the advantages of low density, good corrosion resistance, and excellent thermal and electrical properties [2, 3]. Carbon foam was first produced by Ford in 1964 by the pyrolysis of phenolic resins. It has excellent thermal insulation properties due to its reticular glass carbon structure and highly open porosity. Thus, it was used by the US military in aerospace for high-temperature insulation. It also has more attractive applications in many other fields, such as adsorption, Superior-performance

Supercapacitors, thermal management, catalyst carrier, and electrode materials [4–10]. However, complicated preparation parameters and high production cost are several drawbacks that limit the application and development of carbon foam. In order to obtain a carbon foam having a uniform porous structure, the carbon foam precursor needs to be foamed under high pressure (> 10 MPa) and temperature (~600 °C) [11]. The petroleum-based pitch and the blowing agent are mixed in a reaction vessel, followed by foaming at a high temperature and a high pressure. Finally, the resulting porous pitch foam is pyrolyzed at a high temperature to obtain a carbon foam [12, 13]. A graphite foam is obtained if the temperature reaches 2400 °C. Thus a kind of novel carbon foam is reported, having high porosity (> 99%), and a pore size in the range of 20–100 μm. It has a very low density (~6–8 kg/m³), good flexibility, and improved thermal insulation performance (thermal conductivity $\lambda < 0.1$ W/m K) [14]. The raw material of carbon foam is commercial melamine foam having low cost and can be easily accessed. The new carbon foam has the advantages of low cost and simple manufacturing process.

Aerogel is a novel material with a three-dimensional network structure composed of ultrafine particles. A gaseous dispersion medium is filled in the porous network structure of aerogel. Aerogels generally exhibit a solid state, and more than 90% of the internal volume of the molecules are filled with gas. Aerogels are prepared in two steps; the first

✉ Zhaofeng Chen
zhaofeng_chen@163.com

¹ International Laboratory for Insulation and Energy Efficiency Materials, College of Materials Science and Technology, Nanjing University of Aeronautics and Astronautics, Nanjing 210016, People's Republic of China

² Beijing Spacecrafts, China Academy of Space Technology, Beijing 100080, People's Republic of China

step consists of it synthesized by sol–gel method and the second step consists of drying it by using a suitable drying method in order to minimize the damage of the three-dimensional solid network [15]. Aerogels are highly porous (up to 99%) nanostructure materials owing excellent properties such as high specific surface area (500–1500 m²/g), low density (0.01–0.3 g/cm³), and low thermal conductivity (<0.025 W/m K) [16]. With the development of sol–gel technology and the enhancement of energy-saving awareness, aerogels with light, porous structure have gradually attracted people's attention. It will have more hopeful prospects in many fields, such as acoustic barriers, thermal insulation, supercapacitors and catalytic supports [17–20]. However, most aerogels have the disadvantages of low strength, low toughness, and unstable structure, which significantly limits their application. There are two main techniques for improving the mechanical properties of aerogels; first, by controlling the internal network structure during the preparation process; second, by adding a reinforcing phase to improve the properties. However, currently, there are relatively few studies on carbon foam/aerogel composites. Xin et al. studied the in-situ growth method to prepare a graphene/aerogel composite. Compared to carbon foam, the composite has a specific surface area increased by 55% and a specific capacitance increased by 72% which can be used as a supercapacitor [21]. Zhang et al. investigated pitch-based carbon foam/silica aerogel composite was studied. The compressive strength of the composite is related to carbon foam, and the heat insulation performance is improved [22].

In this study, a new CF/SiO₂ aerogel composite was prepared by a simple and low-cost method including carbonization, sol–gel and drying process. Carbon foam with a three-dimensional network structure obtained by carbonization of melamine foam has low cost and simple processing steps. Also, the CF/SiO₂ aerogel composite preparation by atmospheric drying process has advantages of reduced cost and simple experimental equipment requirements over the supercritical drying technique. Specific mechanical and excellent thermal insulation properties have been reported for the CF/SiO₂ aerogel composite, which will have more expected projections in many fields such as efficient thermal protection system, building energy conservation and energy storage.

2 Experimental process

The melamine foam with a density of 7 kg/m³ and a thickness of 20 mm without flame retardant additives (Henan Zhongyuan Chemical Group) was a kind of flexible foam. The SiO₂ aerogel was prepared by using tetraethyl orthosilicate (TEOS), ethyl alcohol (EtOH) and distilled water as the raw materials, hydrochloric acid as the catalyst for

the hydrolysis reaction, and ammonia as the catalyst for the polycondensation reaction.

The carbon foam was prepared from melamine foam by its carbonization at 350–1100 °C temperature under N₂ atmosphere. The melamine foam was cut into pieces and placed in a tube furnace which was pyrolyzed under the nitrogen atmosphere to obtain carbon foam. Aerogels preparation was carried out in two steps, synthesis by sol–gel and drying under a circumstance of the atmosphere. TEOS distilled water, and EtOH were added to the beaker by 1:5:5 molar ratio and stirred at 60 °C with the help of magnetic stirrer for 20 min, while a small amount 4% of diluted hydrochloric acid was added slowly to promote hydrolysis. Following, adding an appropriate amount (0.05 mol/L) of dilute ammonia was added to adjust the solution's pH around 6–7. After that, the prepared carbon foam sample was immersed in the obtained solution, and then the ammonia water was added dropwise to promote polycondensation process. Finally, after aging and surface modification, the composite sample was dried at 100 °C under a circumstance of atmospheric.

The weight loss of the melamine foam during pyrolysis was analyzed by a thermogravimetric analyzer (NETZSCH STA 449). The microstructure of samples was analyzed by SEM (Hitachi SU8000). The FTIR spectrum (Thermo, Electron Nexus 670) was used to test the changes of the functional groups to verify the reaction mechanisms. The compressive stress of samples was tested by Instron3367 electronic universal testing machine. The thermal conductivity of the samples at ambient temperature was measured by the hot disk (2500s). The Specific surface area and pore size distribution were measured by fully automatic specific surface and porosity analyzer, a specific surface area measuring instrument (ASAP2020).

3 Results and discussion

3.1 Pyrolysis mechanism of carbon foam

Figure 1 shows the TGA curve of the melamine foam in the N₂ atmosphere. There are four stages from room temperature to 900 °C. The melamine foam is hydrophilic and has a high water absorption rate. The weight loss observed during the temperature rise from room temperature to 90 °C was mainly because of the evaporation of adsorbed water. The second stage occurring in the temperature range of 90–370 °C is stable and indicates the stability of melamine foam in this range. Rapid weight loss occurs in the third stage from 370 to 410 °C temperature and the fourth stage from 410 to 1100 °C temperature.

Figure 2 shows the FTIR spectra of melamine foam treated at a different temperature in the N₂ environment. The spectrum of the melamine foam presents characteristic

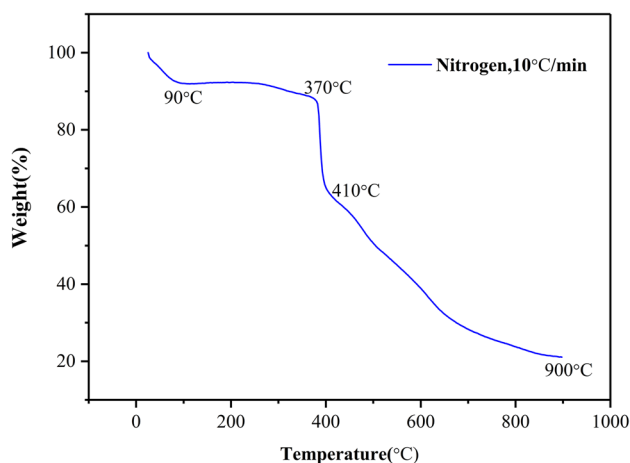


Fig. 1 The TGA curve of the melamine foam

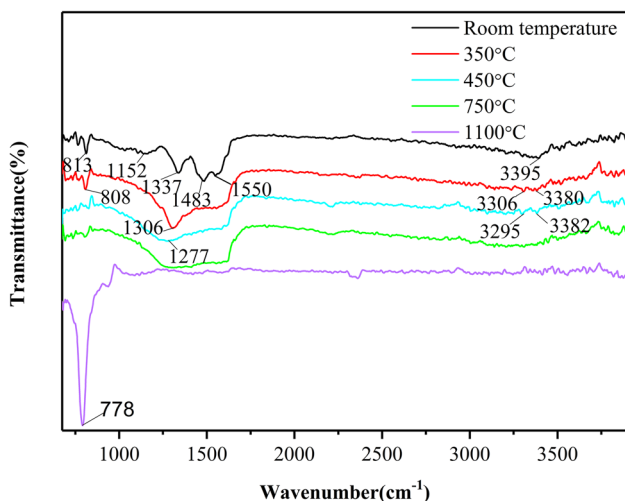


Fig. 2 FTIR spectra of melamine foam treated at different temperature in atmosphere of N_2

peaks at 813 cm^{-1} , 1337 cm^{-1} , and 1550 cm^{-1} that are assigned to the triazine ring. The absorption at 1152 cm^{-1} is a characteristic peak of C–O. The absorption at 1483 cm^{-1} is a characteristic peak of $-\text{CH}_2$ stretching vibration. The absorption at 3395 cm^{-1} is attributed to $-\text{OH}$. The two characteristic peaks of NH_2 are slender and sharp and are coincided with the broad peak of the hydroxyl group. The spectrum of the carbon foam sample treated at $350\text{ }^\circ\text{C}$ is entirely different from the raw melamine foam, as the peaks at 1152 cm^{-1} , 1483 cm^{-1} , 1550 cm^{-1} and 3395 cm^{-1} disappear. For the spectrum, the absorptions at 808 cm^{-1} , 1306 cm^{-1} , 3306 cm^{-1} and 3380 cm^{-1} are the characteristic peaks of the thiotriazinone group in melamine foam. The absorption at 808 cm^{-1} is attributed to $-\text{NH}$. The absorption at 1306 cm^{-1} is attributed to C–N stretching vibration. The

absorptions at 3306 cm^{-1} and 3380 cm^{-1} are attributed to $-\text{NH}_2$. For the spectrum of the carbon foam sample treated at $450\text{ }^\circ\text{C}$, the absorption at 1277 cm^{-1} is attributed to C–N. The absorptions at 3295 cm^{-1} , and 3382 cm^{-1} are attributed to $-\text{NH}_2$. For the spectrum of the carbon foam sample treated at $750\text{ }^\circ\text{C}$, the characteristic peak becomes very wide, and the absorption is attributed to C–N. For the spectrum of the carbon foam sample treated at $1100\text{ }^\circ\text{C}$, the absorption at 778 cm^{-1} is attributed to CH, while the absorption at 2270 cm^{-1} is attributed to $\text{C}\equiv\text{C}$.

The second stage ranges from 90 to $370\text{ }^\circ\text{C}$ temperature. In this stage, decomposition or cracking of the methylene bridge and the ether bond occurs, and the macromolecular chain formed by the crosslinking reaction is broken, while pyrolysis of melamine or residual hydroxymethyl group occurs. The triazine ring structure still exists but becomes more and more unstable. The third stage is from 370 to $410\text{ }^\circ\text{C}$. In this stage, a sharp weight loss (25%) in carbon foam takes place due to the decomposition of the triazine ring. The fourth stage is from 410 to $1100\text{ }^\circ\text{C}$. In this stage, a significant amount of nitrogen is generated in the pyrolysis process due to the denitrification reaction of carbon foam.

3.2 Microstructure of carbon foam and CF/SiO_2 aerogel composite

The microstructural morphology of the carbon foam sample obtained at $750\text{ }^\circ\text{C}$ is shown in Fig. 3a. Carbon foam has a three-dimensional network similar to melamine foam. The connecting node is a triangular ligament with four branches, which are open and connected to each other. Due to volume shrinkage and chemical reaction during pyrolysis, some carbon foam fibers broke at the joint of the triangular ligament, and the carbon foam skeleton structure was damaged to some extent. Average pore diameters of carbon foam were in the range of $40\text{--}80\text{ }\mu\text{m}$. The average pore size of the carbon foam was reduced compared to melamine foam because of the significant volume reduction during the pyrolysis process. Figure 3b shows the model of the carbon foam architecture. The micron-sized dendritic fibers of the carbon foam were interwoven with each other, and the cross-section of the fibers was triangular. The cells of the carbon foam became small, and the fibers became thinner as compared to the melamine foam. During the pyrolysis process, the transition of the polymer to the carbon material occurred, and the elasticity gradually decreased.

Figure 4a shows the micro-morphology of CF/SiO_2 aerogel composite. It is demonstrated that micro-block aerogel was filled with carbon foam cells. The prepared aerogel had cracks but did not have much influence on the composite structure. That is because when the carbon foam sample immersed in the obtained solution, aerogel precursor undergoes a sol–gel process in the cells of carbon foam.

Fig. 3 Micro-morphology and model of sample, **a** Micro-morphology of carbon foam, **b** model of the carbon foam architecture

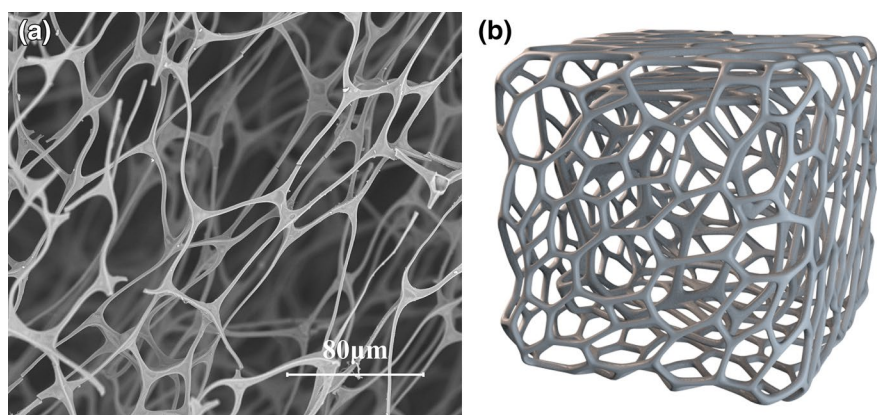
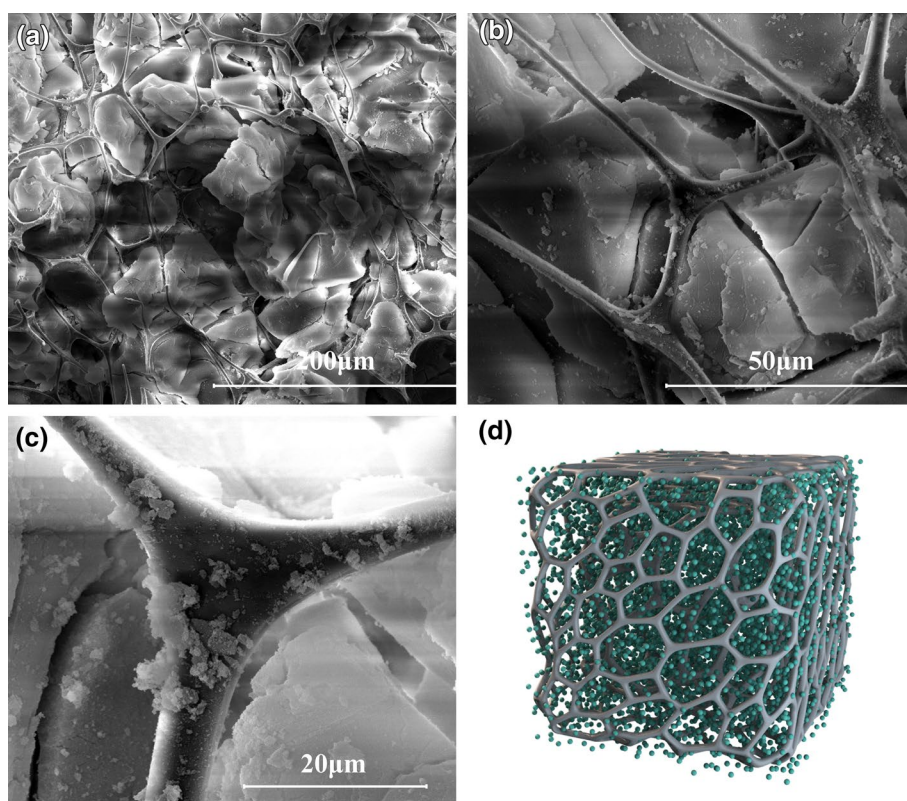


Fig. 4 Micro-morphologies and model of sample, **a–c** Micro-morphologies of CF/SiO₂ aerogel composite, **d** model of the CF/SiO₂ aerogel composite



The three-dimensional network structure of carbon foam maintained their original shape and played a role in supporting the composite as the skeleton. Since the carbon foam easily adsorbed the sol, the organic gel and the carbon foam were combined with each other. The aerogel had been filled with cells of carbon foam, and the filling rate of cells was high. From the high magnification SEM image of CF/SiO₂ aerogel composite (Fig. 4b), the three-dimensional network structure of carbon foam remained intact and had not been damaged due to silica aerogel filling. The silica aerogel, filled with cells of carbon foam maintained a complete block shape, but cracks on the surface were unavoidable due to

drying under ambient pressure. The reason for the crack on the surface is that under a circumstance of the atmospheric drying process, the hydroxyl groups on the surface of the aerogel are condensed with each other. The surface tension causes the internal skeleton structure to shrink, resulting in cracks on the surface. At the same time, the presence of cracks also indicates that SiO₂ aerogel does not have excellent mechanical properties. Not all the cells of the carbon foam were full of aerogel, and some of the cells still have space. Cells of carbon foam are squeezed to a certain extent, but the degree of deformation is not large. The magnified SEM image (Fig. 4c) shows a concave triangle fiber shape

of carbon foam was not tightly bound to the aerogel and there was space between them. A small amount of aerogel remained on the fibers and ligaments of the carbon foam, indicating that the gel was tightly bound to the carbon foam at the beginning of the synthesis. Due to the external vibration, the carbon foam and the aerogel gradually separate, which will have a relatively large impact on the mechanical properties of the carbon foam. Figure 4d shows the model of the CF/SiO₂ aerogel composite architecture.

3.3 Compressive strength of carbon foam and CF/SiO₂ aerogel composite

Figure 5a shows the compressive stress–strain curves of carbon foam. It indicates carbon foam is always in an elastic state when compressed. The maximum compressive stress of carbon foam treated at 750 °C was 0.06 MPa. The strength of carbon foam treated at 1100 °C was too low, and the maximum compressive stress was only 0.01 MPa. If the mechanical properties of the carbon foam are inferior, then it can not function as a skeleton of the composite. The shrinkage of the aerogel will destroy the CF/SiO₂ aerogel composite during the drying process. Although not fully carbonized, the carbon foam treated at 750 °C is highly carbonized. It can be used as a skeleton to support composite. So carbon foam treated at 750 °C was chosen as a precursor for the preparation of composites.

Figure 5b shows the compressive stress–strain curves of CF/SiO₂ aerogel. It indicates that the maximum compressive stress of composite was about 1.0 MPa. When the strain was from 0 to 0.45, the composite was always in an elastic state, and compressive strength raised smoothly and steadily. After the strain reached 0.45, the elastic state changed to a plastic state, and the state of the stress–strain curve was wavy. Pure aerogel prepared by atmospheric drying is brittle, so it has inferior mechanical properties. However, The maximum stress of the composite was much larger than that of carbon foam. On one hand, carbon foam functions as a skeleton to support composite. On another hand, silica aerogel had been full of the cells of carbon foam and tightly

combined with concave triangle fibers. When the composite is subjected to compressive stress, the SiO₂ aerogel matrix begins to produce first cracks, but the deflection of the aerogel crack, the separation of the interface, and the resistance of the carbon foam fibers being pulled out delay the expansion of the crack.

3.4 Thermal conductivity of carbon foam and CF/SiO₂ aerogel composite samples

The thermal conductivity of carbon foam and composites were measured at room temperature (at ambient pressure) and 300 °C (in He atmosphere), respectively. Figure 6 shows the thermal conductivity of samples. At the room temperature, thermal conductivities of carbon foam and CF/SiO₂ aerogel composites were 0.035 W/m K and 0.024 W/m K, respectively. Moreover, the thermal conductivity of CF is 0.12 W/m K. at 300 °C. However, the CF/SiO₂ aerogel composite sample possess a better thermal conductivity compared to the CF at 300 °C, which is 0.057 W/m K. The following aspects can explain the reason why the resulted composite material has better thermal insulation properties.

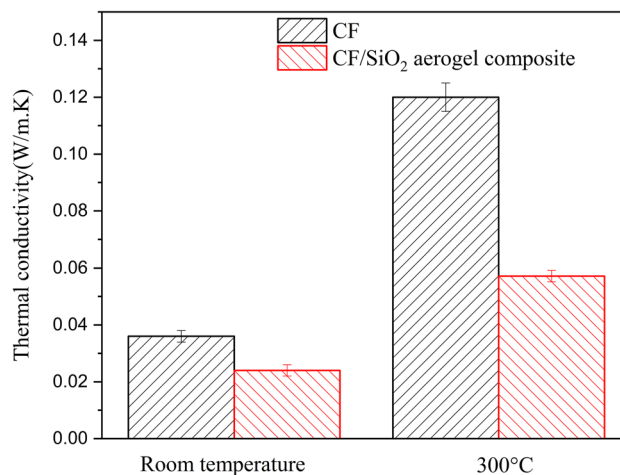


Fig. 6 Thermal conductivities of CF and CF/SiO₂ aerogel composite

Fig. 5 Stress–strain curves of samples, **a** Stress–strain curve of carbon foam, **b** Stress–strain curve of CF/SiO₂ aerogel

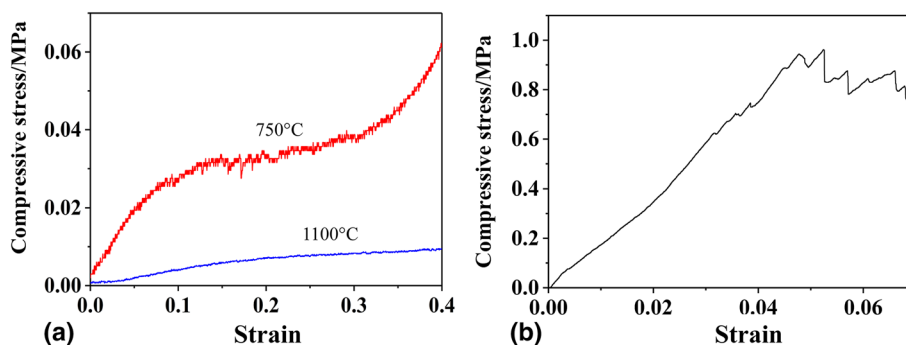


Fig. 7 Schematic illustration of the heat transfer mechanism of samples, **a** CF, **b** CF/SiO₂ aerogel composite

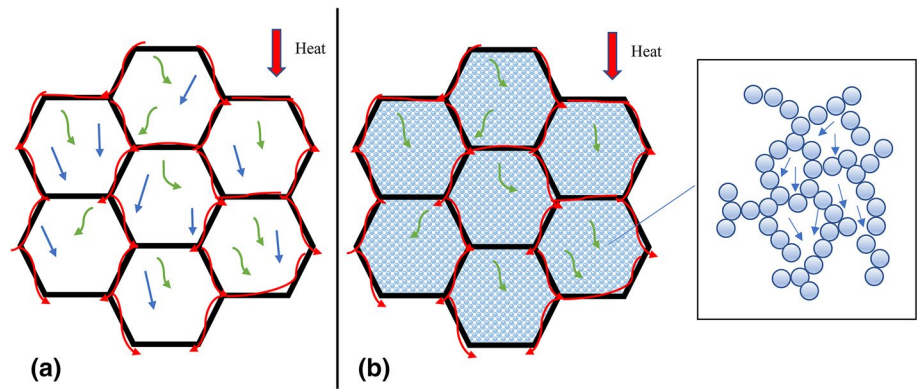


Figure 7 shows the schematic illustration of the heat transferring mechanism in the carbon foam and CF/SiO₂ aerogel composite. Thermal conductivity is mainly due to solid conduction (λ_s), gas conduction (λ_g) and heat radiation (λ_r). At room temperature, the radiative thermal conductivity is negligible. The heat transfer direction is from top to bottom. Red arrows indicate heat transfer along the carbon foam skeleton for solid conduction. Green arrows indicate heat radiant. Blue arrows of Fig. 7a indicates gas conduction in carbon foam, and Fig. 7b blue arrows indicate gas heat conduction in aerogel.

$$\lambda = \lambda_g + \lambda_s + \lambda_r \tag{1}$$

For the gas conduction, the gaseous thermal conductivity in CF/SiO₂ aerogel composite sample can be calculated by the following equations [23].

$$\lambda_g = 0.461(2.25\xi - 1.25) \left(\frac{8k_B T}{\pi m_g} \right)^{\frac{1}{2}} \frac{N_g^0 C_V}{N_A} l_m \tag{2}$$

$$N_g^0 = \frac{P}{k_B T} \tag{3}$$

$$l_m = \frac{1}{0.25S_s \rho_0 / \phi + \sqrt{2} \pi d_g^2 N_g^0} \tag{4}$$

Here, P is pressure (Pa), T is temperature (K), $k_B = 1.38 \times 10^{-23}$ J/K is the Boltzmann constant, $N_A = 6.23 \times 10^{23}$ is the Avogadro constant, ξ is the adiabatic index of gas, m_g is the molecular mass, C_V is the specific heat at constant volume, l_m is the mean free path of the gas molecules, S_s is the specific surface area, ρ_0 is the density, and ϕ is the porosity.

For air, $\xi = 1.4$, $d_g = 3.53 \times 10^{-10}$ m, $m_g = 4.648 \times 10^{-26}$ kg, $C_V = 781.7$ J/(kg K)

$$\lambda_g = \frac{83.4PT^{-0.5}}{0.25S_s \rho_0 / \phi + 4.01 \times 10^4 PT^{-1}} \tag{5}$$

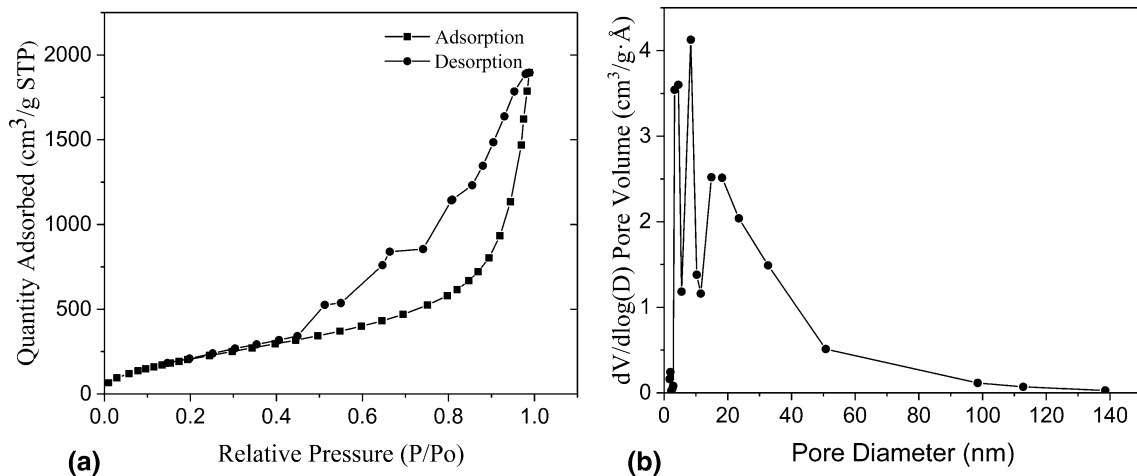


Fig. 8 **a** isothermal nitrogen adsorption and desorption curves of CF/SiO₂ aerogel composite, **b** pore size distribution of CF/SiO₂ aerogel composite

where $S_g = 850.7 \text{ m}^2/\text{g} = 850700 \text{ m}^2/\text{kg}$, $\rho_0 = 180 \text{ kg}/\text{m}^3$, $\phi = 92\%$, $P = 10^5 \text{ Pa}$, $T = 300 \text{ K}$; $\lambda_g = 0.009 \text{ W}/\text{m K}$.

As well known, the mean free path of the air molecules at ambient pressure is about 70 nm. Aerogel is full of cells of carbon foam, and the mean pore size of CF/SiO₂ aerogel composite is tiny. Figure 8a shows isothermal nitrogen adsorption and desorption curves of CF/SiO₂ aerogel composite. The specific surface area of the composite calculated by the BET method is 850.7 m²/g. Figure 8b shows the pore size distribution of CF/SiO₂ aerogel composite. Mean pore size of CF/SiO₂ aerogel composite is 10.4 nm, far less than mean free path of the air molecules at ambient pressure. Pure carbon foam has a huge pore size in the range of 40–80 μm and the specific surface area of carbon foam treated at 750 °C is 270.9 m²/g [14]. According to Eq. (5), We can conclude that the CF/SiO₂ aerogel composite has a small gaseous thermal conductivity compared to carbon foam. The tiny pore size in the aerogel limits the collision between gas molecules and between gas molecules and solid particles. Solid phase SiO₂ content in the aerogel is minimal, and gas is full of the three-dimensional structure. SiO₂ aerogel has a high specific surface area which results in a very low solid thermal conductivity. Aerogel filling in cells of carbon foam dramatically reduces gaseous thermal conductivity, whereas the added solid thermal conductivity is very low, resulting in a significant decrease in total thermal conductivity. At the room temperature, thermal conductivities of carbon foam and CF/SiO₂ aerogel composites were 0.035 W/m K and 0.024 W/m K, respectively. The gas thermal conductivity of the CF/SiO₂ aerogel composite is only 0.09 W/m K ($T = 300\text{K}$, $P = 10^5 \text{ Pa}$), which is far lower than the gas thermal conductivity of the carbon foam. Gas thermal conductivity of carbon foam is about 0.26 W/m K, similar to the thermal conductivity of air.

At 300 °C, the thermal insulation properties of the composite are still very good, up to 0.057 W/m K. Aerogel filled in cells of carbon foam significantly reduce the gaseous thermal conductivity of the composite.

4 Conclusions

(1) Carbonization of melamine foam at 350–1100 °C temperature successfully prepared ultralight and thermal insulation carbon foam. The pyrolysis process of carbon foam is carried out into four stages. In the first stage, the adsorbed water vapor is volatilized by heating. In the second stage, decomposition or cracking of the methylene bridge and the ether bond occurs, and the macromolecular chain formed by the crosslinking reaction is broken, and simultaneous pyrolysis of melamine or residual methylol groups occurs. In the third stage, the triazine ring decomposes. In the fourth stage,

a significant amount of nitrogen is generated during the pyrolysis process due to the denitrification reaction of the carbon foam.

- (2) It indicates that the maximum compressive stress of composite was about 1.0 MPa. Carbon foam functions as a skeleton to support composite. When the composite is subjected to compressive stress, the SiO₂ aerogel matrix begins to produce first cracks, but the deflection of the aerogel crack, the separation of the interface, and the resistance of the carbon foam fibers being pulled out delay the expansion of the crack.
- (3) It indicates that the CF/SiO₂ aerogel composites have a better thermal insulation property at room temperature and 300 °C. Aerogel filling in cells of carbon foam dramatically reduces gaseous thermal conductivity, whereas the added solid thermal conductivity is very low, resulting in a significant decrease in total thermal conductivity.

Acknowledgements The present work was supported by the National Natural Science Foundation of China (Grant No. 51772151) and Jiangsu R&D project (Grant No. BE2017054). This work was also supported by the Priority Academic Program Development of Jiangsu Higher Education Institutions.

References

- N. Gallego, J. Klett, *Carbon* **41**(7), 1461–1466 (2003)
- S. Chen, G. He, H. Hu, S. Jin, Y. Zhou, Y. He, S. He, F. Zhao, H. Hou, *Energy Environ. Sci.* **6**(8), 2435–2439 (2013)
- Y. Wang, Z. Chen, S. Yu, M. Saeed, T. Xu, W. Wang, Y. Pan, J. Eur. Ceram. Soc. **37**(1), 53–59 (2017)
- N. Ohta, Y. Nishi, T. Morishita, Y. Ieko, A. Ito, M. Inagaki, N. Carbon Mater. **23**(3), 216–220 (2008)
- S. He, W. Chen, *J. Power Sources* **262**(9), 391–400 (2014)
- W. Alshaer, S. Nada, M. Rady, E. Barrio, A. Sommier, *Int. J. Therm. Sci.* **89**, 79–86 (2015)
- H. Zhang, Y. Zhou, C. Li, S. Chen, L. Liu, S. Liu, H. Yao, *Carbon* **95**, 388–395 (2015)
- Y. Sun, Q. Wu, G. Shi, *Energy Environ. Sci.* **4**(4), 1113–1132 (2011)
- L. Dimesso, C. Spanheimer, S. Jacke, W. Jaegermann, *J. Power Sources Compos.* **196**(16), 6729–6734 (2011)
- L. Ma, Z. Nie, X. Xi, B. Chen, Y. Chen, *J. Porous Mater.* **20**(3), 557–562 (2013)
- M. Ge, Z. Shen, W. Chi, H. Liu, *Carbon* **45**(1), 141–145 (2007)
- Y. Bao, L. Zhan, C. Wang, Y. Wang, W. Qiao, L. Ling, *Mater. Lett.* **65**(19–20), 3154–3156 (2011)
- T. Li, C. Wang, B. An, H. Wang, *Carbon* **43**(9), 2030–2032 (2005)
- S. Yu, Z. Chen, Y. Wang, R. Luo, Y. Pan, *J. Porous Mater.* **25**(2), 527–536 (2017)
- J. Laskowski, B. Milow, L. Ratke, *J. Non-Cryst. Solids* **441**(1), 42–48 (2016)
- N. Hüsing, U. Schubert, *Angew. Chem., Int. Ed.* **37**(1–2), 22–45 (1998)
- X. Gao, H. Lv, Z. Li, Q. Xu, H. Liu, Y. Wang, Y. Xia, *RSC Adv.* **6**(109), 107278–107285 (2016)

18. M. Reim, W.K.örner,J. Manara, S. Korder, M. Arduini-Schuster, H. Ebert, J. Fricke, *Sol. Energy* **79**(2), 131–139 (2005)
19. J. Feng, D. Le, S. Nguyen, V. Nien, D. Jewell, H. Duong, *Colloids Surf. A* **506**, 298–305 (2016)
20. M. Dawidziuk, F. Carrasco-Marín, C. Moreno-Castilla, *Carbon* **47**(11), 2679–2687 (2009)
21. Z. Xin, W. Li, W. Fang, X. He, L. Zhao, H. Chen, W. Zhang, Z. Sun, *J. Nanopart. Res.* **19**(12), 386 (2017)
22. H. Liu, T. Li, Y. Shi, X. Zhao, *J. Mater. Eng. Perform.* **24**(10), 4054 (2015)
23. S. Zeng, A. Hunt, R. Greif, *J. Heat Transfer* **117**, 758–761 (1995)

Publisher's Note Springer Nature remains neutral with regard to jurisdictional claims in published maps and institutional affiliations.